Supplementary Information:

Tunable Single-Atomic Charge/Spin States of Intercalant Co Ions in a Transition Metal Dichalcogenide

Seongjoon Lim[1], Shangke Pan[1,2], Kefeng Wang[1], Alexey V. Ushakov[3], Ekaterina V. Sukhanova[4], Zakhar I. Popov[4,5], Dmitry G. Kvashnin[4,6], Sergey V. Streltsov[3,7], and Sang-Wook Cheong[1*]

[1] Rutgers Center for Emergent Materials and Department of Physics and Astronomy, Piscataway, NJ 08854, USA

[2]State Key Laboratory Base of Novel Function Materials and Preparation Science, School of Material Sciences and Chemical Engineering, Ningbo University, Ningbo, Zhejiang 315211, China

[3]Institute of Metal Physics, S. Kovalevskaya Street 18, Yekaterinburg 620108, Russia.

[4]Emanuel Institute of Biochemical Physics of RAS, 4 Kosygin Street, 119334, Moscow, Russia

[5]Plekhanov Russian University of Economics, 36 Stremyanny per., 117997, Moscow, Russia

[6]Moscow Institute of Physics and Technology (State University), 9 Institutskiy per., 141701, Dolgoprudny, Moscow Region, Russia

[7]Department of Theoretical Physics and Applied Mathematics, Ural Federal University, Mira Street 19, Yekaterinburg 620002, Russia

*To whom correspondence should be addressed;

Email: sangc@physics.rutgers.edu

1. Computational Details

We found that the type of long-range magnetic ordering does not affect the valence state of Co ions in $Co_{1/3}NbS_2$. Although the total energy of the antiferromagnetic structure is lower by ~3 meV per formula unit than the ferromagnetic one, we used the ferromagnetic order for simplicity. Thus, all the theoretical calculations and the STM simulations described below concern only structural vacancies, deformations, or various substitutions of one ion by another without any contrast of magnetic origin. Moreover, the simulated STM response based on our *ab initio* calculation is not sensitive to the magnetic structure of $Co_{1/3}NbS_2$ unless one assumes magnetized tip, which is consistent with our STM observation (using non-magnetic tip) seeing no magnetic contrast.

We also checked the influence of spin-orbit coupling on Co ions carried out by various GGA+U+SOC calculations. In all the calculations the orbital moment is on the order of $\sim 10^{-4}$ μ_B and therefore spin-orbit interaction could be neglected in the current analysis. One may also find that the total energy in GGA+U+SOC approximation does not depend on the spatial spin orientation of Co ions. Although changes in simulated STM images are obtained in the case of a supercell with four Co ions when the spin moment of one Co ion is perpendicular to others, such a pattern was not obtained in the experiment. Thus, we do not consider the noncolinear situation and assume that all spin moments on Co ions have the same orientation. We also verified that the findings stay unchanged whether the correlation effects (Hubbard U; up to 2 eV) are included in the calculation or not. All the considerations above can be justified further by consistency of all the STM observed defects matching with the simulated STM images based on the calculation scheme.

In the simulated STM images, the distance from the STM tip to the sample surface was set to be equal to 3.0 Å. Negative and positive bias voltage (BV) images were obtained by consideration of the charge distribution in the energy range from $+E_0$ eV to the Fermi energy or from $-E_0$ eV to the Fermi energy, respectively. We considered two values of E_0 (0.05 eV and 0.15 eV) which were selected based on the experimental parameters.

1.1. **Electronic Structure of Bulk $Co_{1/3}NbS_2$**

We start theoretical consideration with analysis of the bulk $Co_{1/3}NbS_2$ electronic structure. Formally there are two possibilities: (i) both Co and Nb ions might adopt 3+ valence state or (ii) Co ion is 2+, while Nb is nominally $3\frac{1}{3}$ (the system is metallic). Our GGA+U calculations show that the second scenario realizes in bulk and there are 7.2 *d*-electrons within Co atomic sphere, i.e. Co is 2+, which is consistent with the further analysis of the occupation matrix as well as the previously reported results[1,2]. The different valence state of Co and Nb is due to the larger principal quantum number of Nb 4*d* states. As a result, Nb 4*d* states lie higher in energy than the Co *3d* bands, and it makes unfavorable to have the same oxidation states for Co and Nb ions.

Co ions are in the high-spin configuration, $t_{2g}^5 e_g^2$, with the local magnetic (spin) moment of 2.45 μ_B, reduced from nominal 3 μ_B corresponding to S=3/2 due to covalency. The partial densities of states projected to each atomic species are presented in **Figure S1**.

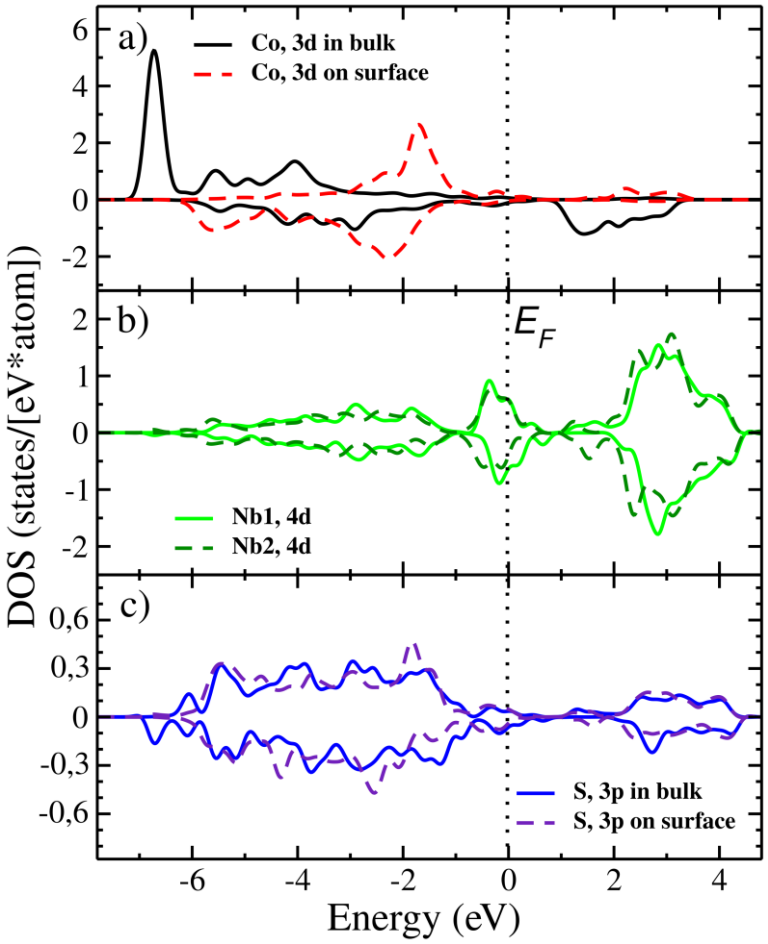

Figure S1. **Partial Densities of States of $Co_{1/3}NbS_2$ Obtained by GGA+U Calculations. a.** Densities of *3d* states of Co^{2+} (d^7) in bulk (black solid line) and Co^{1+} (d^8) in layer 1 of (0001) surface (red dashed line). **b.** Densities of 4*d* states of two structurally inequivalent Nb1 (green solid line) and Nb2 (dark green dashed line). **c.** Densities of 3*p* states of S ions in bulk (blue solid line) and in layer 2 of (0001) surface (purple dashed line). See Fig. 1 of the main text for layer numbering of the structure. The sign of the graph indicates projection to two opposite spin directions and the Fermi energy is shown as the vertical dotted line.

One may observe a large hybridization between Co 3*d*, Nb 4*d*, and S 3*p* states. The trigonally distorted configurations of NbS_6 prisms and CoS_6 octahedra lift the degeneracy of Co and Nb t_{2g} manifolds and split both of them onto a_{1g} and e_g^{π} states. The common-face type sharing of triangular S ions between NbS_6 and CoS_6 results in a strong overlap between the a_{1g} orbitals of Co and Nb along the *c* direction. There exist prominent Nb 4*d* metallic bands at the

Fermi level, and hybridization brings also some Co a_{1g} states towards the Fermi level. The shift of Co a_{1g} states is crucial for STM experiments, which on one hand probe the states close to the Fermi energy but on another hand are susceptible to only states of ions at the surface (i.e. Co atoms).

2. Theoretical Analysis of STM Data on Co-Terminated (0001) Surface

We simulated various types of defects including various vacancies and substitutional defects. We used 3×3×1 supercells of $Co_{1/3}NbS_2$ for most of the atomistic defect models, and 6×6×1 supercell is employed in the case of Co divacancy located in layer 1.

2.1. Pristine Surface of $Co_{1/3}NbS_2$

It is interesting that the electronic state of Co ions on (0001) surface is very different from what we have in the bulk. While the total number of electrons is just slightly larger (7.6 electrons) than that of bulk, analysis of the occupation matrix definitely shows that the electronic configuration is d^8, i.e. Co^{1+}, with the reduced local magnetic (spin) moment of 1.93 μ_B. The larger number of *d* electrons at the surface is related to the specific surface termination of Co ions having only half of S ions after cleaving, so they are located on top of a sulfur triangle without any S ions above. The reduced coordination let the crystal field splitting between the t_{2g} and the e_g states almost disappear. Using Wannier-function projection technique[3] we obtained the reduced crystal field splitting of Co ion from ~1.2 eV for bulk to ~0.3 eV for surface. The reduced splitting stimulates electron redistribution from Co e_g^σ orbitals and Nb orbitals towards Co a_{1g} states, and it makes Co closer to Co^{1+} oxidation state.

The simulated STM image for pristine (0001) surface of $Co_{1/3}NbS_2$ is shown in **Figure S2**b. The triangular arrangement of bright spots at the positions of Co ions agrees with the experimental results (**Figure S2**c and Main Text **Figure 1**). It is worth mentioning that STM measurements are mostly sensitive to the electronic structure of surface in general, but it is dramatically demonstrated in our STM images showing only the triangular Co ion lattice without any hint of subsurface S or Nb lattice symmetries. It could be expected that the strong surface-sensitive response will be due to the a_{1g} orbitals of Co ions with electron density extending perpendicular to the surface. (Fig. 2b in the main text) However, as we will show below other states (not only of Co ions) also affect electron density distribution through hybridization with Co *3d* orbitals.

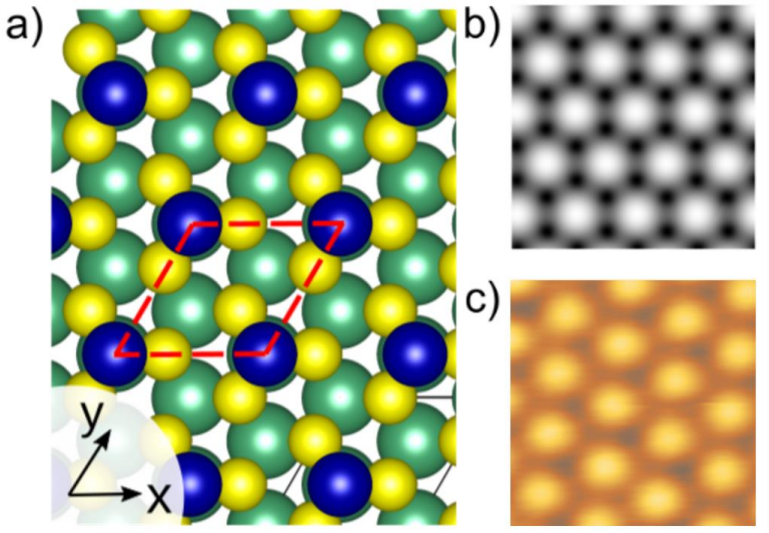

Figure S2. Pristine $Co_{1/3}NbS_2$ (0001) Surface. **a.** Atomic structure and the considered unit cell highlighted by red dashed line. (Blue: Co, Teal: Nb, and Yellow: S) **b.** Simulated and **c.** Experimental STM image (BV = -0.15 eV).

In the meantime, one of the most interesting questions is: "How it is possible to change the oxidation state of Co at the surface from 1+ (d^8) to 2+ (d^7) state?" The switching could be done

by means of applying voltage since d^7 Co^{2+} state is locally stable and the energy difference between d^8 and d^7 is small. There comes an advantage of GGA+U approach that Hubbard U correction deepens most of the local minima of density functional. We have taken advantage of the GGA+U characteristic to stabilize solution on a model where every fourth Co ion set to be 2+. (Technically, this was done by applying a constraint on the magnetization on first few iterations) **Figure S3b** and **Figure S3c** compare the simulated STM image using the GGA+U approach and the measurement, and they are agreed on the bright glowing feature of Co^{2+} ion at the center. The energy of the solution is about 0.13 eV/Co higher than the ground state and the difference is in fact on the order of the bias voltage used to induce change from Co^{1+} to Co^{2+} in the experiment.

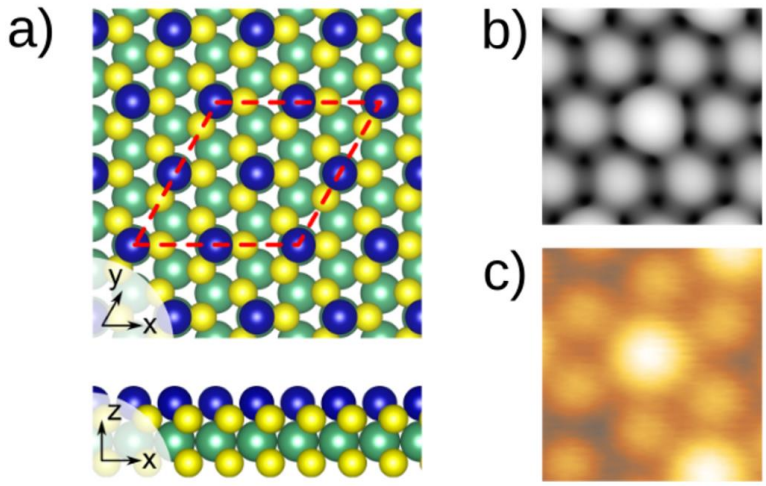

Figure S3. $Co_{1/3}NbS_2$ Surface with Central Co Excited to 2+ Valence State. **a.** Atomic structure and the considered unit cell highlighted by red dashed line **b.** Simulated and **c.** Experimental STM images (BV = -0.15 eV).

2.2. Experimentally Observed Structural Defects in $Co_{1/3}NbS_2$

The isolated Co vacancy located at layer 1 is the most frequently observed type of defects on $Co_{1/3}NbS_2$ samples. The simulated STM image is shown in **Figure S4b**, which fits well with the experimental image (**Figure S4c**). A dark spot can be observed in the experimental STM image which can be explained by the absence of Co a_{1g} orbital due to the Co vacancy.

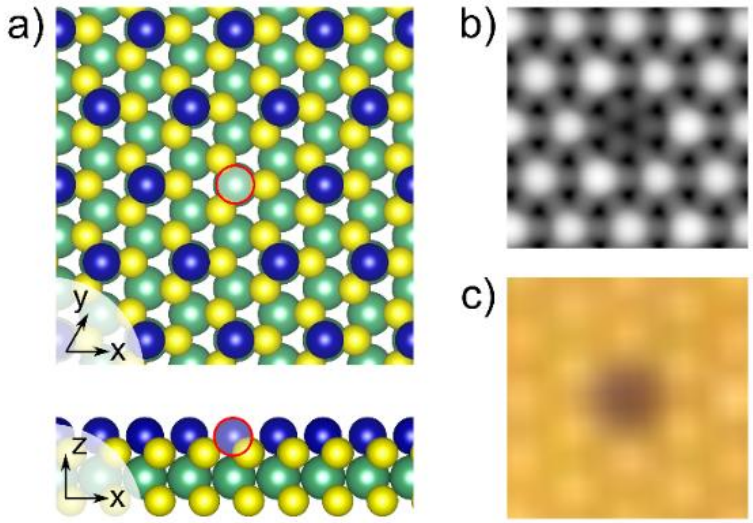

Figure S4. $Co_{1/3}NbS_2$ Surface with Co Atom Monovacancy. **a.** Atomic structure with a vacant Co site in layer 1 marked by the red circle. **b.** Simulated (BV = -0.15 eV) and **c**. Experimental STM images of the Co monovacancy.

In the experimental images, we can also observe Co atom divacancies that show consecutive two dark spots. (compare **Figure S5b** and **Figure S5c**) Another interesting defect structure related to Co divacancy is the reconstructed triangular-patterned dark spots such as one shown in **Figure S5f**. The reconstruction moves one of the neighbor Co ion towards the center as described by the red arrow in **Figure S5d**, and the theoretical simulation reproduces the observed defect as compared in **Figure S5e** and **Figure S5f**. The energy of the relaxed structure (with Co atom shift) is lower than the initial configuration by 10 meV per unit cell and therefore it is possible to expect such reconstruction at a finite temperature.

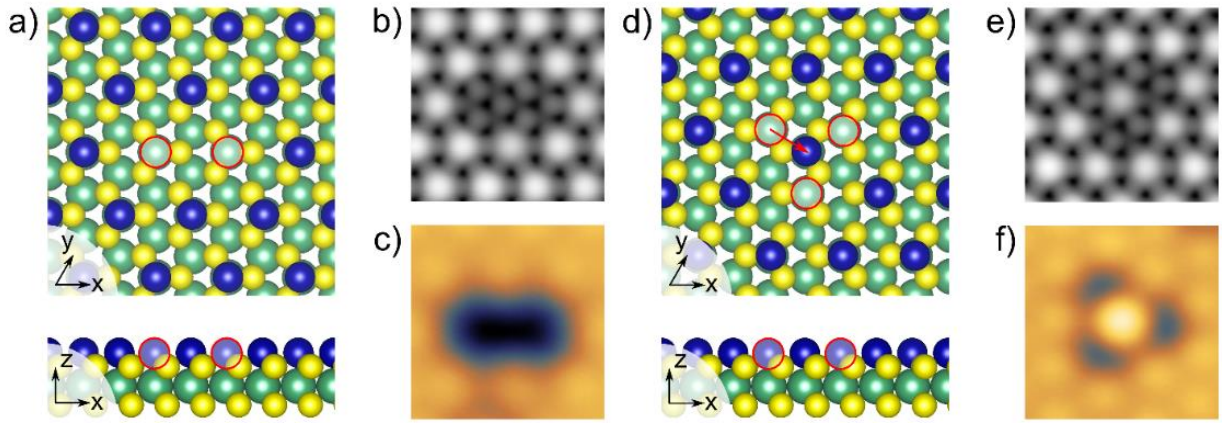

Figure S5. Original and Reconstructed Structures of $Co_{1/3}NbS_2$ with Co Divacancy. **a,d**. Atomic structures with the vacancies marked by red circles. The red arrow in (d) indicates the movement of one Co ion towards the center. **b,e.** Simulated and **c,f.** Experimental STM images (BV = -0.15 eV) of the original and the reconstructed divacancy structure, respectively.

Another interesting defect that can be observed in the experimental STM images is a bright triangular spot as shown in **Figure S6c**. We found two possible structural configurations which can be related to this defect: Nb atom vacancy and iodine atom substitution.

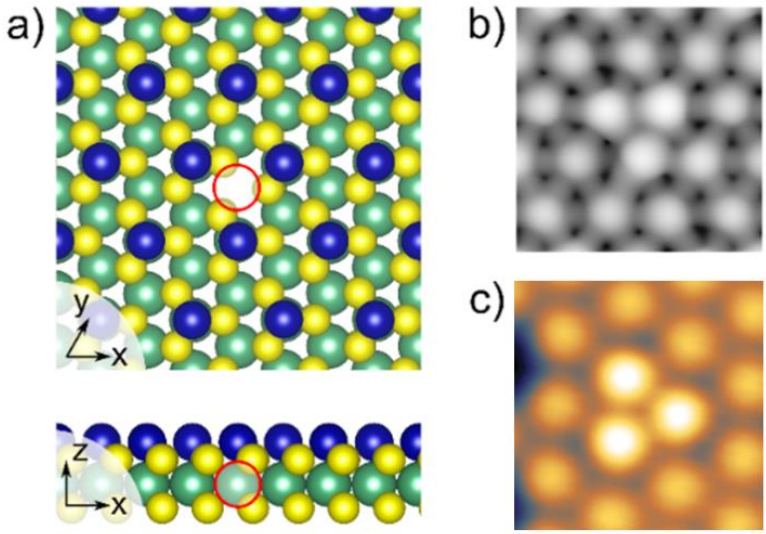

Figure S6. $Co_{1/3}NbS_2$ Surface with a Nb Vacancy in Layer 3. **a.** Atomic structure with Nb vacancy marked by the red circle located in layer 3. **b.** Simulated (BV = -0.15 eV) and **c**. Experimental STM images of the Nb vacancy.

Since iodine gas was used as a transport agent during the chemical vapor transport growth, we also considered iodine atoms substitution as a possible defect in the $Co_{1/3}NbS_2$ atomic structure. The considered structures and obtained theoretical STM images are presented in **Figure S7**. In the case of an Nb atom substituted by an iodine atom, which is located underneath the center of triangular Co atoms (**Figure S7c**) we also can observe bright triangular feature in the simulated STM image. In contrast, if iodine substitution is located directly under the Co atom, then a significant surface reconstruction is observed in the calculation: The iodine atom shifts toward layer 5 Co while Co atom from the layer 1 moves to the Nb atom position (**Figure S7a**).

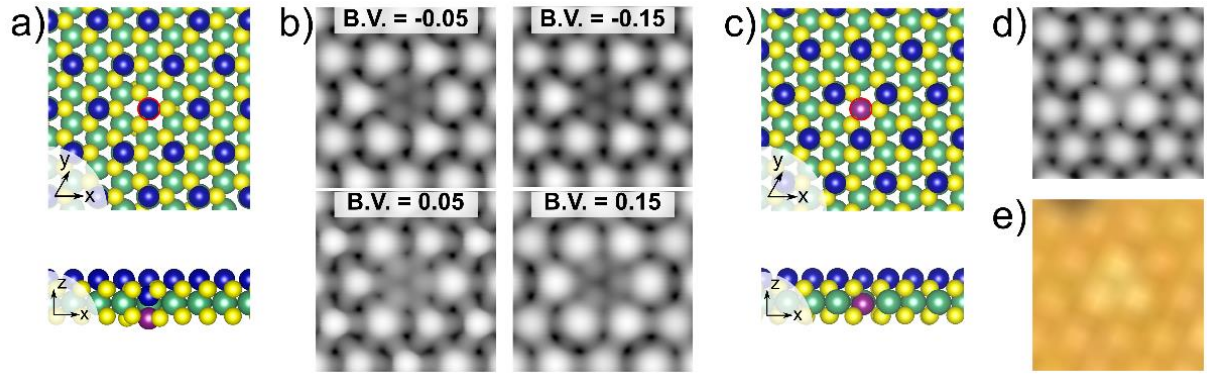

Figure S7. Two Configurations with Nb Atom Substituted by Iodine Atom. a. Iodine substituted Nb in layer 3 located directly under a layer 1 Co. The red circle shows the position of the substituted Nb atom in layer 3, and purple color indicates the iodine atom. **b.** Simulated STM images of the defect model in (a) with various BVs. **c.** Iodine substituted Nb in layer 3 located at the center of triangular layer 1 Co ions. **d.** Simulated STM image of the model in (c). **e.** Candidate STM measurement corresponding to the model in (c).

While we see that most of the textures observed in the experimental STM images can be explained by either of a vacancy or a substitution, there is one feature that required more extended type of defect structure. Such a defect shows a corona-like depression surrounding a Co ion as shown in **Figure S10d**. Although we have considered several types of extended

defect types, such as Co monovacancy in layer 5 (**Figure S8a**), Co divacancy in layer 5 (**Figure S8c**), and S vacancy in layer 2 (**Figure S9a**), they failed to give a consistent simulated STM image of the corona-like feature. It is rather clear from the symmetry consideration that the corona-like feature centered at the Co ion in layer 1 can only be related to any defect type preserving C3 symmetry around the Co atom at the surface. Therefore, the forementioned Co monovacancy, divacancy, and S vacancy that break the C3 symmetry cannot reproduce the C3 symmetric corona-like feature. One might see the AB type stacking shown in **Figure 1a** of the main text to realize how difficult it is to preserve the C3 symmetry from any simple defects.

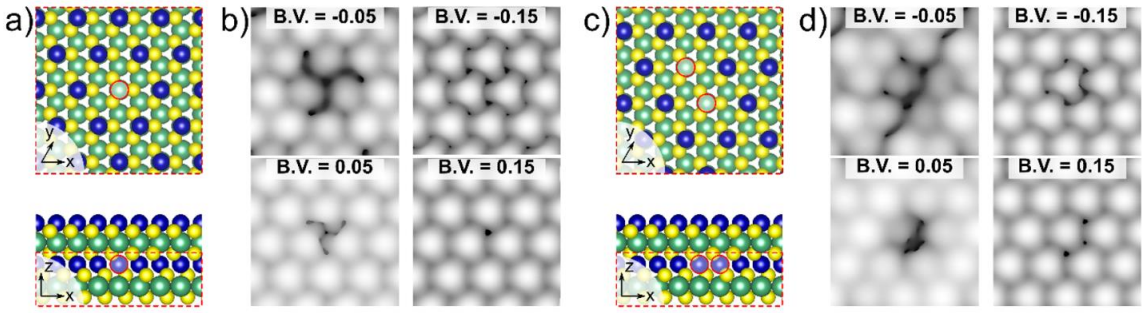

Figure S8. Atomic Structure with Co Mono and Divacancies Located in Layer 5. a,c. Atomic structure of Co monovacancy (a) and divacancy (c) in layer 5. The red dashed box shows the displayed regions of the *xy* plane model, and the red circles indicate the positions of monovacancy. **b,c.** Simulated STM images with different values of the bias voltage of considered structures, respectively. The red dashed boxes show the range of presented atoms by omitting the first four layers in the *xy* plane view. The red circles indicate vacant Co sites in layer 5.

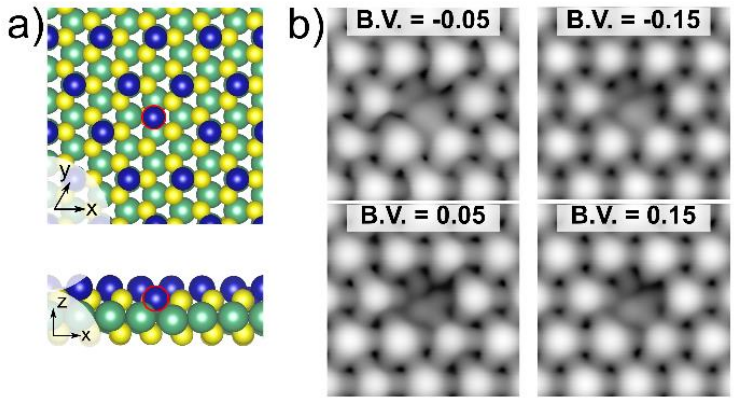

Figure S9. $Co_{1/3}NbS_2$ Surface with S atom Vacancy in Layer 2. a. Atomic structure of the defect model with S vacancy in layer 2. The missing S position is indicated with the red circle while the position is filled with the moved Co ion after calculation. **b.** Simulated STM images with various BVs.

Instead of the simple defects, we considered a more extended Co trivacancy in layer 5, which will be yet simplest defect model with preserved C3 symmetry (**Figure S10a).** One might see that the central spot becomes smaller and a darker region surrounding the central Co atom appears in the simulated STM images in **Figure S10b** and **Figure S10c**, which reproduce the corona-like feature. The existence of Co trivacancy underneath draws considerable charge density decrease around the central Co atom without breaking C3 symmetry. The microscopic description of this effect is rather straightforward. Metallic bands at the Fermi level mostly have Nb *4d* (refer **Figure S1b**), but a strong hybridization between a_{1g} orbitals of Co and $3z^2$-r^2 orbitals of Nb looking directly to each other brings Co a_{1g} states to E_F. These are the states, which are measured in the STM experiment. Removing some atoms in the Co layer 5 changes the electronic structure of Nb and these changes spread to the surface. We observe that the charge redistribution on the a_{1g} orbital of the Nb atom due to a vacancy is~10%, which is enough to be detected by STM.

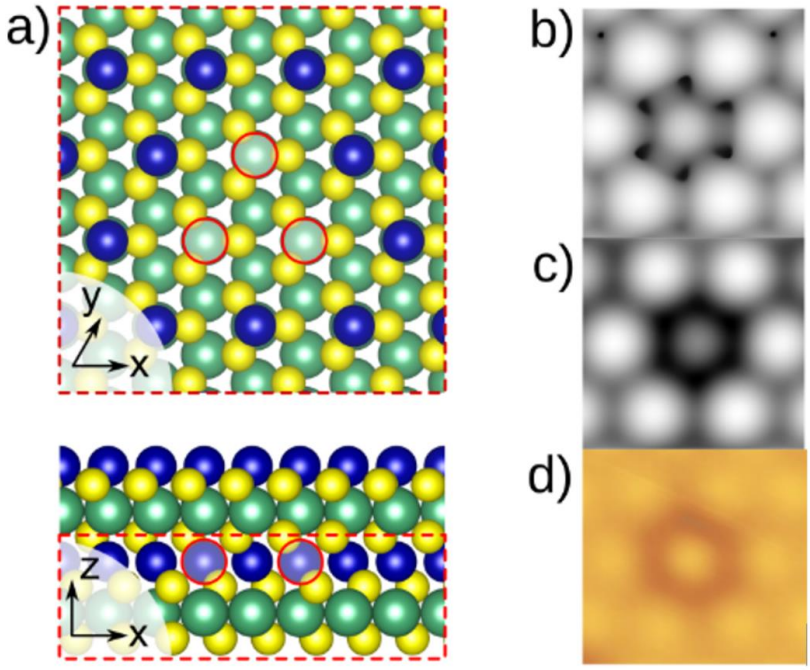

Figure S10. $Co_{1/3}NbS_2$ Atomic Structure with Co Trivacancy Located in Co layer 5. a. Atomic structure of the trivacancy. The red dashed boxes show the range of presented atoms by omitting the first four layers in the *xy* plane view. The three red circles are missing Co atoms in layer 5. **b.c.** Simulated STM images (BV = -0.15 eV) with distances to tip equal to 3 Å (b) and 4 Å (c), respectively. **d.** Experimental STM image of the trivacancy structure.

The simulated STM images of other possible structural defects (Substitution of S ion by I ion in layer 2/4; Shift of Co ion in layer 1) are presented in **Figure S11** and **Figure S12**. They are not observed experimentally yet, nonetheless theoretical predictions allow their formation.

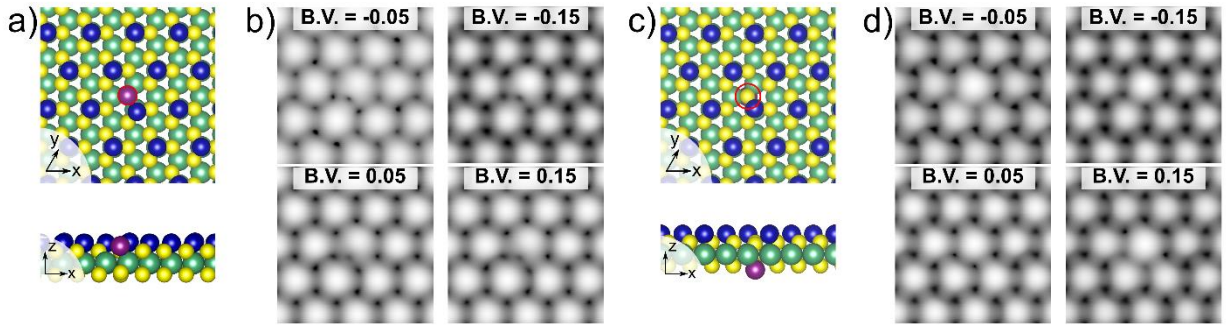

Figure S11. $Co_{1/3}NbS_2$ Surface with S Atom Substituted by I Atom in Layers 2 and 4. a,c. Atomic structures. **b,d.** Simulated STM images with various BVs.

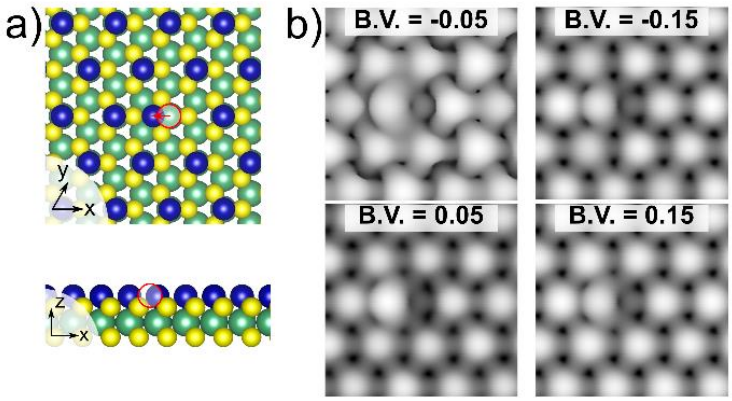

Figure S12. $Co_{1/3}NbS_2$ surface with Co ion shifted in layer 1. a. Atomic structure. **b.** Simulated STM images with various BVs.

2.3. Comparison of Co-Centered Defects in Height Profiles

After finding all the structural defect types and their corresponding experimental STM images, we could compare three somewhat similar defect types that are centered around a surface Co ion. They are the metastable charged state of Co^{2+}, Co substitution of Nb in layer 3, and Co trivacancy in layer 5. Especially Co substitution of Nb has a slight protrusion compared to the pristine Co ion state, and careful comparison is required to distinguish it from the charged Co^{2+} state. Since the details of STM profile can be affected by STM tip orbital condition, the analysis is based on a data obtained from the same STM topographic image without any trace of tip condition change. The charged Co^{2+} state can be distinguished from the other two defects by showing markedly different lateral extension and vertical protrusion as shown in **Figure S13**.

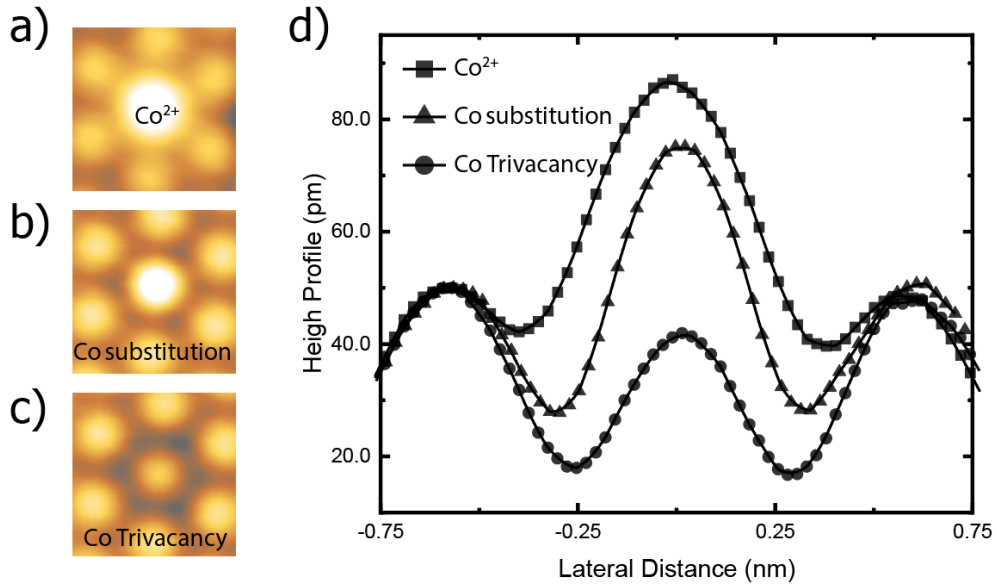

Figure S13. Comparison of STM Heigh Profiles of **Three Co-centered Defects. a.** Metastable charged Co^{2+} state. **b.** Co substitution of Nb in layer 3 **c.** Co trivacancy in layer 5. **d.** Height profiles of the three types of defects. The curves are normalized to the height of the Co on the left side.

3. Statistical Analysis of the Metastable Charged State

3.1. Estimation of the Decay Constant

Since we have noticed the manipulated metastable charged Co^{2+} states resulting in restoration to the ground state, we tried to estimate the time scale of such a decaying process. To observe multiple charged Co^{2+} states at the same time, we have created many charged states within a certain area. Although the point pulsing process described in the main text is highly efficient in making a single charged Co^{2+}, the process involving the maximum current exceeding the measurement limit of our current amplifier (>10 nA) was not appropriate for the massive manipulation. Instead, we increased the BV to -500mV without increasing the tunneling current from the nominal imaging setpoint current ~10pA. We kept the elevated BV during a raster scanning within an area of 100 nm^2, where we found several hundreds of charged Co^{2+} sites with some unstable signal changes right after. The unstable signal has gone after the initial few minutes (~3 mins), and then consecutive images are analyzed to track the change in the number of charged Co^{2+} sites.

STM images in **Figure S14** show the change of the charged Co sites at each 14 mins of time interval, where we indicated the charged sites with black dots. The change in the number of charged sites revealed simple exponential decay behavior as presented in **Figure S15**, which is fit with decay constant t_0 of about 2,600 sec. Since we had to ignore the first few images with the unstable signal, we can consider that some of the charged states change back to the ground state more violently with much shorter time scale. So, it is likely that there exists distinguished shorter decay time scale for ions near vacancies, which is evidenced from some images showing unstable changes near vacancies as in **Figure 1h** (main text, red dashed circles).

Therefore, the long decay time scale of 2,600 seconds can also likely be affected by a surrounding defect structure, and the dependence on the exact surrounding environment is subject to further investigation in the future.

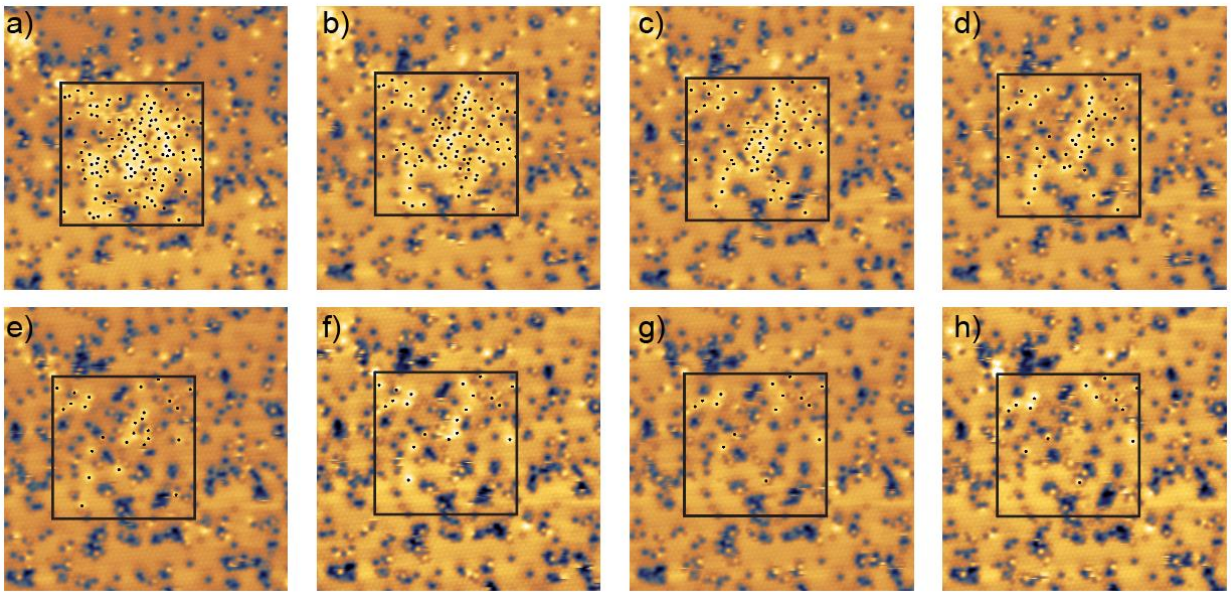

Figure S14. Series of STM Images Showing Decay of Charged Co^{2+} ions. a-h. Center area indicated by the black square (10×10 nm^2) was initially raster scanned at an elevated BV of -500mV to create multiple charged Co^{2+} sites. Then 20×20 nm^2 area was monitored at a nominal imaging BV to see the change of charged Co^{2+} numbers in every 14 mins. The black dots mark the identified charged Co^{2+} sites.

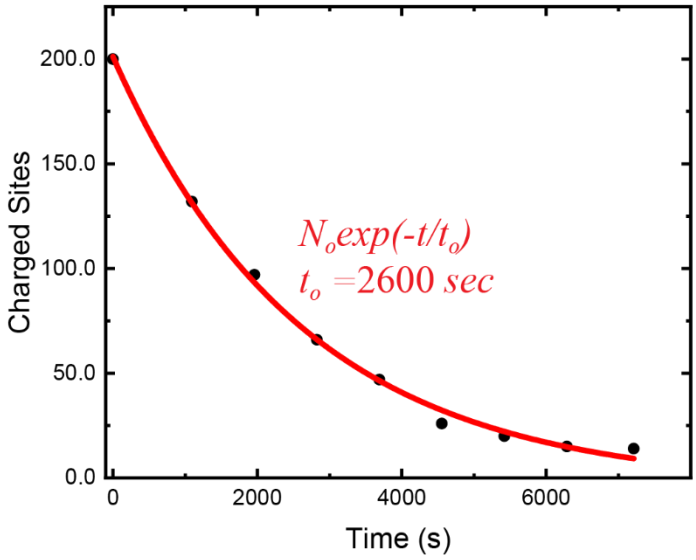

Figure S15. Exponential Decay of Charged Co^{2+} Ions with Time. The numbers are counted from the series of STM images partly presented in **Figure S14** and the curve is fitted with single exponent decay function shown with the red line. The fitted half-life decay time t_0 was estimated to be 2600 secs.

3.2. Number of Electrons to Induce Charged Co

The change of Co ion valence state from 1+ to 2+ is caused by loss of one electron, and the movement of the electron can be either to the tip or the sample. And the direction will be determined by the BV applied between the tip and the sample likewise the electrons tunneling through the vacuum gap. The number of electrons required to induce such an electron hopping can be a measure of quantum yield of the overall charging process, and its dependence on the BV and STM tip height can be valuable information to understand the precise microscopic mechanism. Although the BV dependence could not be resolved in detail because of various unwanted change of Co status at higher BV, such as lateral movement of Co ion itself or sticking to the tip end, we could stably measure the time to induce a charging event at a relative moderate BV and tunneling current instead.

At sample biases around ±200 meV, the time to observe a Co charging event showed an easy-to-measure range from several seconds to several tens of seconds. The required time and the

number of electrons to induce a single charging event is measured for more than 20 events for each combination of BV and tunneling current and summarized in **Table S1**. It can be noticed that the quantum yield increases with higher tunneling current as expected, and that applies both of the polarities. The measured ~10^{10} electrons per a single charging event is 3 orders of magnitude higher than the reported value of single atom charging performed on thin insulating layer[4], which requires further investigation on the role of the van der Waals gap in stablizing the charged state.

Table S1 Statistics of Charging Processes at Positive and Negative BV.

Sample Bias (mV)	**Tunneling Current (pA)**	**Time (Sec)**	**Number of Electrons (10^{10} e^-)**
-200	300	9.1 ± 8.2	1.7
-200	500	3.5 ± 2.3	1.1
200	300	14.6 ± 12.9	2.7
200	500	5.8 ± 3.3	1.8

References

1. Parkin, S. S. P., Marseglia, E. A. & Brown, P. J. Magnetic structure of Co1/3NbS2and Co1/3TaS2. *J. Phys. C Solid State Phys.* **16**, 2765–2778 (1983).
2. Nakayama, M., Miwa, K., Ikuta, H., Hinode, H. & Wakihara, M. Electronic Structure of Intercalation Compounds of CoxNbS2. *Chem. Mater.* **18**, 4996–5001 (2006).
3. Korotin, D. *et al.* Construction and solution of a Wannier-functions based Hamiltonian in the pseudopotential plane-wave framework for strongly correlated materials. *Eur. Phys. J. B* **65**, 91–98 (2008).
4. Repp, J., Meyer, G., Olsson, F. E. & Persson, M. Controlling the Charge State of Individual Gold Adatoms. *Science* **305**, 493–495 (2004).